

Real poles with opposite-sign residues in the non-perturbative quark propagator

R. Alkofer^a, M.N. Ferreira^b, A.S. Miramontes^c, J.M. Morgado^c, J. Papavassiliou^c

^a*Institute of Physics, University of Graz, NAWI Graz, Universitätsplatz 5, Graz, 8010, Austria*

^b*Instituto de Física, Universidade Federal do Rio Grande do Sul, Porto Alegre, 150151, Brazil*

^c*Department of Theoretical Physics and IFIC, University of Valencia and CSIC, Valencia, E-46100, Spain*

Abstract

We investigate the analytic structure of the quark propagator in the Landau gauge by dynamically coupling the standard gap equation to the non-perturbative quark-gluon vertex. Employing the full vertex basis, we demonstrate that for sub-GeV time-like momenta, the proper inclusion of the underlying dynamics leads to a pair of real poles with opposite-sign residues. In particular, in stark contradistinction to the results obtained in widely used approximations, we see no sign of complex conjugate poles. This distinctive analytic structure evades conceptual shortcomings frequently associated with complex conjugate poles while remaining fully compatible with the aspects of color confinement related to positivity violation. Crucially, this novel behavior is governed by a dominant triplet of vertex form factors: the tree-level component, the anomalous chromomagnetic moment, and a component we label as “spin-momentum curvature”. By gradually tuning the individual strengths of these components, we demonstrate that while they contribute in distinct ways to the quark propagator, their joint action is vital for stabilizing the system. Together, they place the low-lying poles onto the real axis while producing a robust constituent quark mass of 350 MeV.

1. Introduction

During the past decades, significant progress has been achieved in mapping fundamental QCD correlation functions in the Euclidean domain, driven by a successful synergy between functional methods and gauge-fixed lattice simulations [1–10]. However, even in the most studied gauge, the Landau gauge, the quantitative understanding of these functions away from the space-like axis, crucial for both practical computations and the scrutiny of color confinement, remains largely incomplete; for related works, see *e.g.*, [11–32].

Within this context, exploring the analytic structure of the unquenched quark propagator is of fundamental importance. Phenomenological applications have long benefited from standard truncation schemes which, while providing a fair description of various hadronic properties [10, 33–52], endow the quark propagator with a pair of complex conjugate poles [53–57]. These poles have been occasionally interpreted as suggestive of confinement [58–60]; nevertheless, it remains unclear whether this contentious feature represents an intrinsic property of the theory or an artifact of omitting subdominant vertex components [11, 31, 61]. Evidently, a conclusive resolution of this question requires a full-fledged dynamical analysis, where the structure of the vertex is derived from its own underlying field equations.

In the present work, we take a significant step in this direction by solving the fully coupled system composed of the gap equation for the up quark and the corresponding Schwinger-Dyson equation (SDE) for the quark-gluon vertex. In the Landau gauge employed here, the latter consists of eight tensorial elements and their attendant form factors, which for simplicity are evaluated in the *soft-gluon limit*. We demonstrate that the inclusion of this complete vertex structure converts the

typical complex conjugate poles into a pair of real poles with residues of opposite-sign, as in the recent study of [61], which has been conducted within the quenched approximation in the chiral limit.

Crucially, this novel behavior is governed by a dominant triplet of vertex form factors: the transversely projected tree-level component (TLC) λ_1 , the chirality-violating anomalous chromomagnetic moment (ACM) λ_4 [62, 63], and the chirally symmetric λ_7 , for which we coin the term “spin-momentum curvature” (SMC) due to its explicit dependence on the momentum commutator $[p, k]$.¹ By systematically tracking the migration of the propagator poles, we expose a delicate balance within this key triplet of form factors. While the TLC with unchanged strength² alone yields real poles but underestimates the constituent mass (~ 180 MeV), the inclusion of the ACM at full strength produces substantial mass enhancement (~ 550 MeV) but generates complex conjugate poles. At this point, the inclusion of the SMC leads to the restoration of the initial pole structure. Specifically, by introducing a scaling parameter to gradually dial in the strength of the SMC, we reveal a critical threshold past which the complex conjugate poles are diverted back onto the real axis. At their full physical strengths, the TLC, ACM, and SMC perfectly balance the system, yielding real poles while generating a robust constituent quark mass of ~ 350 MeV. Crucially, on the space-like side, this complete vertex structure alters the momentum dependence of the mass

¹Here p and k denote the two quark momenta, see below. The form factor correspondence with [61] is $\Gamma^{(1)} \leftrightarrow$ TLC, $\Gamma^{(6)} \leftrightarrow$ ACM, while the SMC is a linear combination of $\Gamma^{(1)}$, $\Gamma^{(2)}$, and $\Gamma^{(4)}$.

²Note that in all studies based on the rainbow-ladder truncation, the strength of the TLC is either phenomenologically determined or artificially enhanced.

function compared with simpler vertex models. This modification brings the resulting constituent mass into much closer agreement with the recent precise lattice results of [64].

The final upshot of this analysis is that the complex conjugate poles seem to emerge because the gap equation kernel is unbalanced w.r.t. the chiral symmetry respecting TLC, the chirality violating ACM, and the chiral symmetry preserving SMC. Specifically, when the required strength is concentrated within a restricted vertex structure, the geometry of the propagator poles is destabilized. Instead, when the kernel support is properly distributed among all relevant form factors, as dictated by the full dynamics, (i) the complex conjugate poles disappear, (ii) the correct mass scale is reproduced, and (iii) the momentum dependence of the constituent quark mass function is favorably modified.

2. Quark propagator and quark-gluon vertex

In this section we provide a concise overview of the principal components and general notation employed throughout the present work. Note that, in general, we formulate the main equations in Minkowski space, and recast them into Euclidean hyperspherical coordinates for the final numerical treatment.

2.1. The basic equations

We work in the Landau gauge, where the gluon propagator, $\Delta_{\mu\nu}^{ab}(q) = -i\delta^{ab}\Delta_{\mu\nu}(q)$, assumes a completely transverse form

$$\Delta_{\mu\nu}(q) = P_{\mu\nu}(q)\Delta(q^2), \quad P_{\mu\nu}(q) = g_{\mu\nu} - q_\mu q_\nu / q^2. \quad (1)$$

We denote the up quark propagator by $S^{ab}(p) = i\delta^{ab}S(p)$ [65], and employ the standard parametrization

$$S(p) = \sigma_v(p^2)\not{p} + \sigma_s(p^2), \quad S^{-1}(p) = A(p^2)\not{p} - B(p^2), \quad (2)$$

with

$$\sigma_v(p^2) = \frac{1}{A(p^2)[p^2 - M^2(p^2)]}, \quad \sigma_s(p^2) = M(p^2)\sigma_v(p^2), \quad (3)$$

where $M(p^2) = B(p^2)/A(p^2)$ is the renormalization-group invariant constituent quark mass. The momentum evolution of these functions is governed by the gap equation, shown in the upper panel of Fig. 1, which reads

$$S^{-1}(p) = S_0^{-1}(p) - i\Sigma(p), \quad (4)$$

where $S_0(p)$ denotes the tree-level quark propagator, while

$$\Sigma(p) = -\frac{4g^2}{3} \int_q \gamma_\mu S(p+q) \bar{\Gamma}^\mu(q, p, -p-q) \Delta(q^2), \quad (5)$$

is the quark self-energy, g is the QCD gauge coupling, and $\int_q := (2\pi)^{-4} \int d^4q$ represents a suitably regularized integration over virtual momenta. For later convenience we define $p^2\Sigma_A(p^2) = \text{Tr}[\not{p}\Sigma(p)]$ and $p^2\Sigma_B(p^2) = \text{Tr}[\Sigma(p)]$.

The key element entering in the self-energy $\Sigma(p)$ of Eq. (5) is the transversely projected quark-gluon vertex, defined as

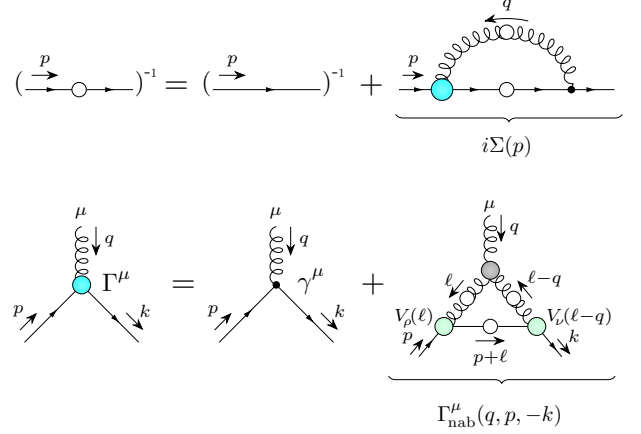


Figure 1: Upper panel: Diagrammatic representation of the quark gap equation. Lower panel: The SDE of the quark-gluon vertex in the SV approximation. White circles denote full propagators, the cyan circle represents the full quark-gluon vertex, the green circles indicate the combination $V(q^2)\gamma^\mu$, while the grey circle stands for the full three-gluon vertex.

$\bar{\Gamma}^\mu(q, p, -k) = P^{\mu\nu}(q)\Gamma_\nu(q, p, -k)$, whose tree-level expression is given by $\bar{\Gamma}_0^\mu(q) = P^{\mu\nu}(q)\gamma_\nu$.

In general kinematics, $\bar{\Gamma}^\mu(q, p, -k)$ is spanned by eight tensor structures [66],

$$\bar{\Gamma}^\mu(q, p, -k) = \sum_{i=1}^8 \lambda_i(q, p, -k) \bar{\tau}_i^\nu(p, -k), \quad (6)$$

where $\bar{\tau}_i^\nu(p, -k) = P_\nu^\mu(q)\tau_i^\nu(p, -k)$, and the tensor basis is given by $\tau_1^\nu = \gamma^\nu$, $\tau_2^\nu = (k+p)^\nu$, $\tau_3^\nu = (\not{k} + \not{p})\gamma^\nu$, $\tau_4^\nu = (\not{k} - \not{p})\gamma^\nu$, $\tau_5^\nu = (\not{k} - \not{p})(k+p)^\nu$, $\tau_6^\nu = (\not{k} + \not{p})(k+p)^\nu$, $\tau_7^\nu = -\frac{1}{2}[\not{k}, \not{p}]\gamma^\nu$, $\tau_8^\nu = -\frac{1}{2}[\not{k}, \not{p}](k+p)^\nu$.

Note that, since $\bar{\tau}_4^\mu = P_\nu^\mu(q)(\not{k} - \not{p})\gamma^\nu = P_\rho^\mu(q)i\sigma^{\rho\nu}q_\nu = i\sigma^{\mu\nu}q_\nu$, the component $\lambda_4(q, p, -k)$ corresponds to the ACM, a tensorial quark-gluon coupling akin to the loop-induced Pauli term in QED.

In addition, as we will see in Sec. 4.3, the element $\lambda_7 \bar{\tau}_7^\nu$ affects crucially the analytic structure of the quark propagator. The commutator $[\not{k}, \not{p}]$ in $\bar{\tau}_7^\nu$ acts as a measure of local geometric curvature in the space of the quark and anti-quark momenta. By virtue of $\bar{\tau}_7^\nu = -\frac{1}{2}P_\nu^\mu(q)[\not{k}, \not{p}]\gamma^\nu = -iP_\nu^\mu(q)\sigma^{\alpha\beta}k_\alpha p_\beta \gamma^\nu$, this curvature structure is mapped directly onto the spin tensor $\sigma^{\alpha\beta}$, linking the spatial distortion to the internal orientation of the particle. We will therefore refer to this vertex component as “spin-momentum curvature” (SMC). This terminology is further supported by the fact that the SMC contains three Dirac matrices, constituting a higher-rank tensor within the Clifford algebra (corresponding to the basis tensor $R^{(2),\mu}$ in [61]). Consequently, the SMC is structurally distinct from the other three chirally symmetric form factors, $\bar{\tau}_{1,5,6}^\nu$, which contain only a single Dirac matrix and therefore represent standard vector-like quark-gluon couplings.

2.2. The SDE of the quark-gluon vertex

The momentum evolution of the $\lambda_i(q, p, -k)$ is controlled by the quark-gluon vertex SDE. The most complete “one-loop

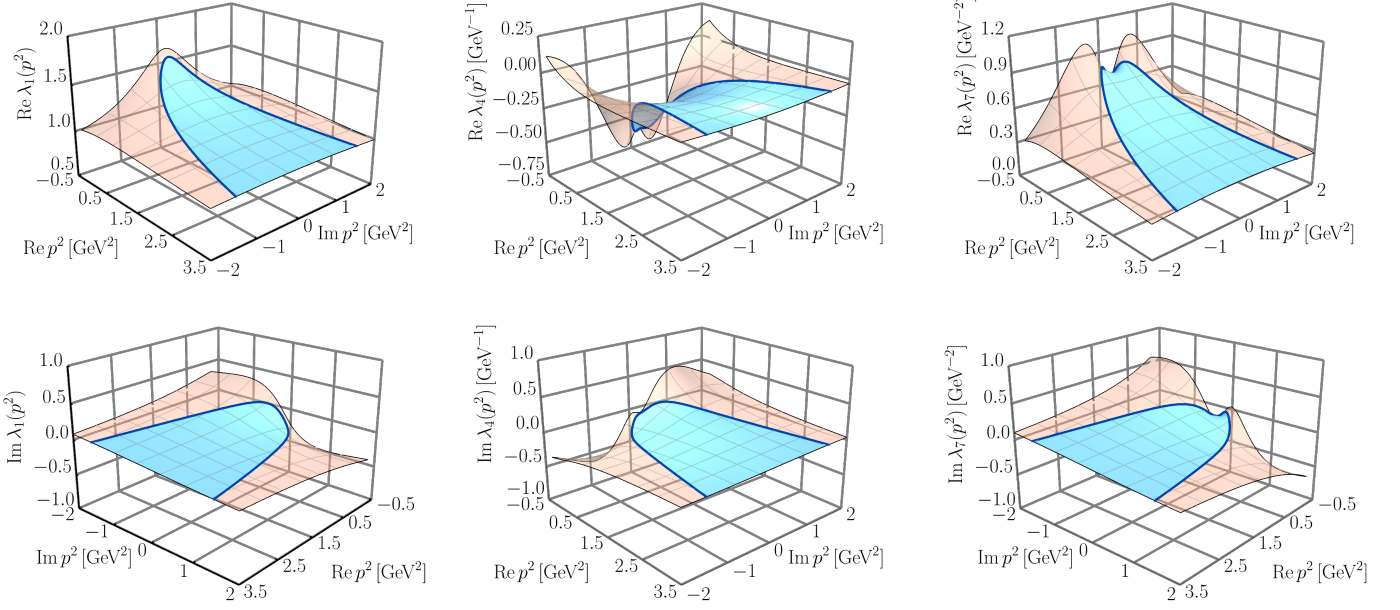


Figure 2: Real (top) and imaginary (bottom) parts of the quark-gluon vertex form factors $\lambda_1(p^2)$, $\lambda_4(p^2)$, and $\lambda_7(p^2)$; displayed in the left, middle and right panels, respectively. The blue parabolas delimit the region of validity of the Euclidean formulation, where the numerical calculations have been performed [32]. The pale orange surfaces denote the result of the extrapolation by means of the Schlessinger Point Method (SPM).

“dressed” form of this SDE [61, 66–68] has been obtained within the three-particle irreducible (3PI) effective action formalism [68–72], and contains two “one-loop dressed” diagrams, traditionally referred to as “Abelian” and “non-Abelian”, see *e.g.*, Fig. 2 in [61]. Since it is well-known that the contribution of the “Abelian” graph is rather negligible, in what follows we will only consider the “non-Abelian” term.

This 3PI-SDE will be further simplified, motivated by the recent analysis of [73–75]. Specifically, all quark-gluon vertices inside the “non-Abelian” diagram are replaced by a single form factor, proportional to γ_μ , which depends solely on the momentum of the incoming gluon. Thus, inside the diagram $\bar{\Gamma}_{\text{nab}}^\mu$ in Fig. 1 we substitute $\Gamma^p(\ell, p, -\ell_1) \rightarrow V(\ell^2)\gamma^p$ and $\Gamma^v(-\ell_2, \ell_1, -k) \rightarrow V(\ell_2^2)\gamma^v$ where $\ell_1 = p + \ell$ and $\ell_2 = \ell - q$.

The function $V(q^2)$ is determined by first solving the 3PI-SDE maintaining full quark-gluon vertices inside $\bar{\Gamma}_{\text{nab}}^\mu$, and isolating the form factor $\lambda_1^{\text{3PI}}(q, p, -k)$, multiplying the classical tensor γ_μ . Then, the slice of $\lambda_1^{\text{3PI}}(q, p, -k)$ corresponding to the symmetric configuration, $q^2 = p^2 = k^2$, is singled out, and identified with $V(q^2)$, *i.e.*, $V(q^2) = \lambda_1^{\text{3PI}}(q^2, q^2, q^2)$.

Under this approximation, the vertex SDE, shown in the lower panel of Fig. 1, is given by

$$\bar{\Gamma}^\mu(q, p, -k) = \bar{\Gamma}_0^\mu(q) + \bar{\Gamma}_{\text{nab}}^\mu(q, p, -k), \quad (7)$$

with

$$\bar{\Gamma}_{\text{nab}}^\mu = \frac{3ig^2}{2} \int_\ell \bar{\Gamma}_0^v(\ell_2) S(\ell_1) \bar{\Gamma}_0^p(\ell) \bar{\Gamma}_{vp}^\mu V(\ell_2^2) \Delta(\ell_2^2) V(\ell^2) \Delta(\ell^2), \quad (8)$$

where $\bar{\Gamma}^{\mu\nu\rho}(q, r, p) = P_\mu^\mu(q) P_\nu^\nu(r) P_\rho^\rho(p) \Gamma^{\mu\nu\rho}(q, r, p)$ denotes the transversely-projected three-gluon vertex. According to various studies [76–82], an excellent approximation to $\bar{\Gamma}^{\mu\nu\rho}(q, r, p)$ may

be obtained by setting

$$\Gamma^{\mu\nu\rho}(q, r, p) = L_{\text{sg}}(s^2) [g^{\nu\rho}(r-p)^\mu + g^{\mu\rho}(p-q)^\nu + g^{\mu\nu}(q-r)^\rho], \quad (9)$$

with $s^2 = (q^2 + r^2 + p^2)/2$, and the form factor $L_{\text{sg}}(s^2)$ given by Eq. (A1) and Tab. II of [83].

Within this approximation, the final expressions for the eight $\lambda_i(q, p, -k)$ are straightforwardly obtained from Eq. (8), after suitable projection and subsequent integration (no iterative procedure required).

2.3. The soft-gluon limit of the quark-gluon vertex

We simplify the analysis further, by considering the so-called “soft-gluon (sg)” limit of the quark-gluon vertex [32], namely

$$\bar{\Gamma}^\mu(q, p, -k) = \sum_{i=1}^8 \lambda_i^{\text{sg}}(p^2) P_i^\mu(q) \tau_i^\nu(p, -k). \quad (10)$$

Note that we maintain the tensorial structure *intact*, while the attendant form factors $\lambda_i^{\text{sg}}(p^2) := \lim_{q \rightarrow 0} \lambda_i(q, p, -k)$ depend on a single kinematic variable, namely p^2 .

The equations that determine the $\lambda_i^{\text{sg}}(p^2)$ can be derived by taking the $q \rightarrow 0$ limit of the corresponding projections of the SDE in Eq. (7), namely

$$\lambda_i^{\text{sg}}(p^2) = \delta_{i1} + \lim_{q \rightarrow 0} \text{Tr} \left[\underbrace{\mathcal{P}_{i,\mu}(q, p, -k) \bar{\Gamma}_{\text{nab}}^\mu(q, p, -k)}_{\lambda_{i,Q}^{\text{sg}}(p^2)} \right], \quad (11)$$

where the projectors $\mathcal{P}_i^\mu(q, p, -k)$ are given in Eq. (3.9) of [66]. The explicit integral expressions obtained through this procedure are given in Eq. (3.9) of [32].

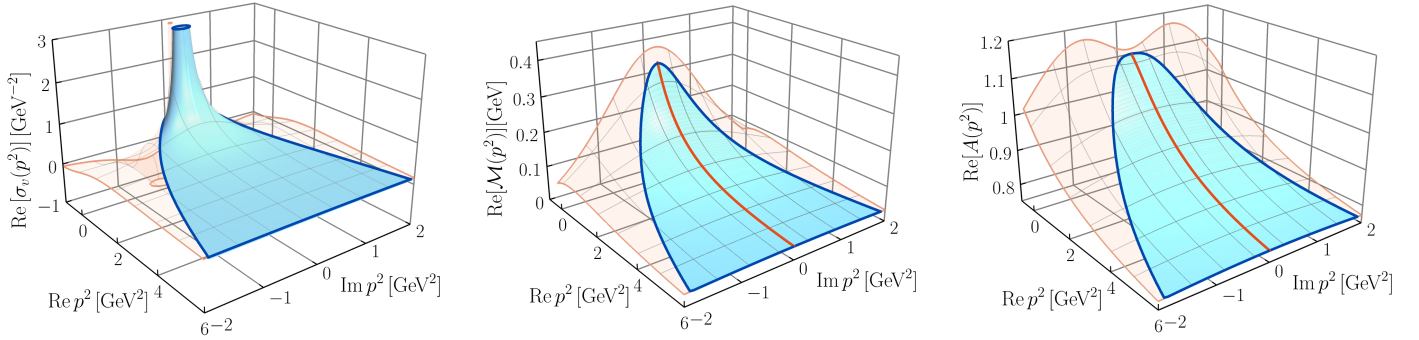


Figure 3: Plots of the real parts of the Dirac component $\sigma_v(z)$ (left panel), the constituent quark mass function, $\mathcal{M}(p^2)$ (middle panel), and the dressing function $A(p^2)$ (right panel) in the complex momentum plane; all components of the quark-gluon vertex were included in their derivation. The blue parabolae delimit the region where numerical calculations were performed, while the pale orange surfaces represent the SPM extrapolations of the corresponding results.

Note that, within this approximation, an ambiguity arises when λ_i^{sg} is inserted in the gap equation: the argument of λ_i^{sg} could be considered to be either p^2 or $(p+q)^2$. Evidently, if the momentum p^2 is used, the $\lambda_i^{sg}(p^2)$ would appear outside the q -integration in Eq. (5). Instead, we choose the representative momentum to be $(p+q)^2$, such that the strength of $\lambda_i^{sg}((p+q)^2)$ is integrated over inside the gap equation, as happens when the full momentum dependence is retained. This choice, in turn, guarantees the ultraviolet finiteness of the results, once the subtractions dictated by the renormalization procedure have been duly carried out, as described below.

2.4. Renormalization

The renormalization of the system of equations composed of Eqs. (4) and (7) is carried out according to the procedure outlined in Sec. V of [74]. In particular, after the introduction of the appropriate renormalization constants (see *e.g.*, Eq. (3.13) in [66]), we employ the version of the momentum-subtraction scheme [84–86] known as $\overline{\text{MOM}}$ [66, 83, 87–89]. This scheme is defined using as reference precisely the soft-gluon limit of the quark-gluon vertex, namely through the prescriptions [87]: $\Delta_R^{-1}(\mu^2) = \mu^2$, $A_R(\mu^2) = 1$, $B_R(\mu^2) = m_r(\mu^2)$ and $\lambda_{1,R}^{sg}(\mu^2) = 1$. In addition, the multiplicative renormalization of the quark self-energy is implemented through the expedient employed in [74] (see also [90–92]), leading to the effective replacement $Z_1\gamma_\mu \rightarrow V_\mu(q)$, where Z_1 is the renormalization constant of $\overline{\Gamma}_\mu(q, p, -k)$.

Thus, one arrives at the renormalized system of equations

$$\begin{aligned} S_R^{-1}(p) &= \not{p} - m_r - i[\Sigma_R(p^2) - \Sigma_R(\mu^2)], \\ \lambda_{i,R}^{sg}(p^2) &= \lambda_{i,Q}^{sg}(p^2) + [1 - \lambda_{i,Q}^{sg}(\mu^2)]\delta_{i1}, \end{aligned} \quad (12)$$

with $\lambda_{i,Q}^{sg}(p^2)$ defined in Eq. (11), and

$$\Sigma_R(p^2) = -\frac{4g^2}{3} \int_q \gamma_\mu V(q^2) S_R(p+q) \overline{\Gamma}_R^\mu(q, p, -p-q) \Delta_R(q^2). \quad (13)$$

3. Solving the coupled system in the complex plane

In this section we focus on the treatment of the system given by Eq. (12) in the complex plane. We emphasize that this prob-

lem contains a single external momentum, namely p , which enters both in the gap equation (first of Eq. (12)), as well as in the vertex form factors $\lambda_i^{sg}(p^2)$ (second of Eq. (12)). It is this particular momentum that will be complexified, $p^2 \rightarrow z$, while the virtual (integration) momenta remain real (Euclidean). Note in particular, that the momentum p may be channeled exclusively through the quark propagator of the graph $\overline{\Gamma}_{\text{nab}}^\mu$ in Fig. 1; therefore, all other components of $\overline{\Gamma}_{\text{nab}}^\mu$ are evaluated at Euclidean momenta, where lattice results are available.

3.1. Inputs

The solution of the system Eq. (12) requires four external ingredients, all of which are defined at $\mu = 2$ GeV.

(i) For the Landau-gauge gluon propagator, we employ the fit to the $N_f = 2$ lattice data of [93, 94], given in Eq. (A1) of [83] and shown in the top-left panel of Fig. 6 in [74].

(ii) For the form factor $L_{sg}(s^2)$, we use the fit to the lattice data of [95] reported in Eq. (A1) of [83]. The corresponding form factor is displayed in the top-right panel of Fig. 6 in [74].

(iii) For the function $V(q^2)$ we adopt the parametrization given in Eq. (6.5) of [74], shown in the bottom-right panel of Fig. 6 therein.

(iv) Finally, for the renormalized current quark mass we employ $m_r = 50$ MeV; we will comment on this choice in Sec. 4.

3.2. Details of the numerical treatment

The system of equations given by Eq. (12) is reformulated in Euclidean space following standard conversion rules; see *e.g.*, Sec. IV. B and App. A in [66]. Then, the external momentum is complexified, employing the parametrization $p^2 \rightarrow z = x + iy$, while the integration (loop) momenta remain real and positive.

Our numerical procedure solves simultaneously for the $A(p^2)$, $B(p^2)$ and $\lambda_i^{sg}(p^2)$, by treating them as a system of coupled equations, iterating until overall convergence is achieved.

Specifically, the numerical algorithm is organized as follows:

(i) In order to commence the procedure, an initial expression for the quark propagator that appears in the integral of Eq. (8) is required. We find it convenient to employ as our initial “guess” function the solution of the gap equation obtained in [47]; the corresponding $A(p^2)$ and $\mathcal{M}(p^2)$ are shown in Fig. 4

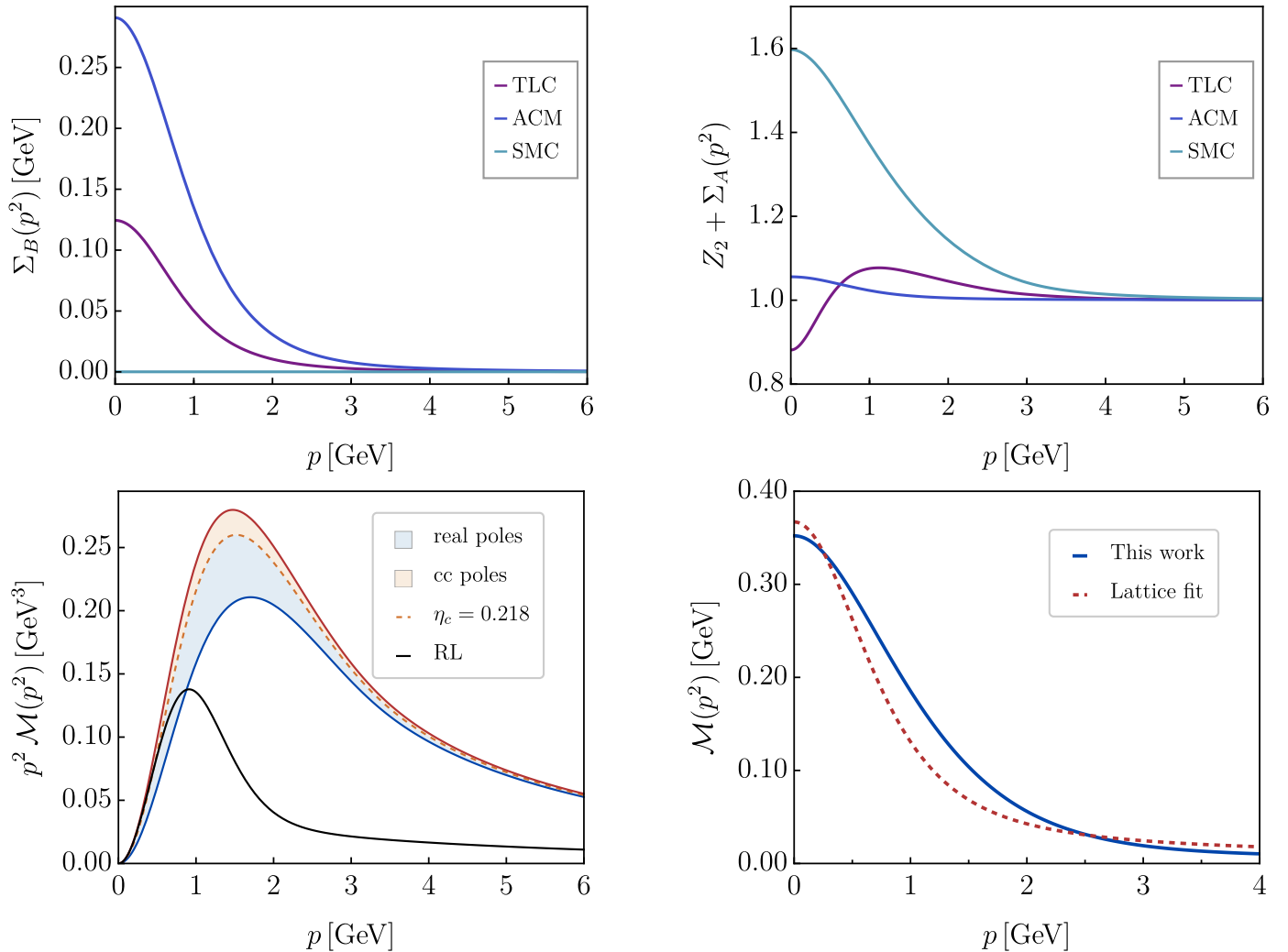


Figure 4: Upper panels: Individual contributions of the TLC, ACM, and SMC to the quark propagator functions $B(p^2)$ and $A(p^2)$, obtained by solving the gap equation with only the respective vertex component retained. The upper left panel clearly illustrates that the dominant contribution to $B(p^2)$ —and thus to dynamical mass generation—originates from the ACM, while the SMC does not contribute to $B(p^2)$ at all. Conversely, the largest contribution to the dynamical dressing of $A(p^2)$ is driven by the SMC. Together, the ACM and SMC induce a distinct momentum dependence in the mass function $\mathcal{M}(p^2)$ compared to the TLC-only result. Lower left panel: The product $p^2 \mathcal{M}(p^2)$ compared with the corresponding rainbow-ladder (RL) truncation (black line); the solid red line isolates the TLC and ACM structures, while the solid blue line displays the full triad with the SMC included. Lower right panel: Comparison of the full triad result with the lattice parametrization of [64].

therein. Solutions obtained from other standard versions of the gap equation should be equally appropriate for initializing the calculation.

(ii) Next, we determine the location of the first singularities of the input propagator in the complex plane, denoted by $p_s^2 = R_s e^{i\theta_s}$. These singularities define the boundary of the region where the standard Euclidean formulation remains valid [32], and consequently the maximal domain where the vertex form factors can be computed. This region corresponds to the parabolic domain defined through the equation $y^2 = ax + b$, with $a = 4R_s \cos^2(\theta_s/2)$ and $b = 4R_s^2 \cos^4(\theta_s/2)$.

(iii) The form factors $\lambda_i^{sg}(p^2)$ are then computed within the allowed domain through direct numerical integration.

(iv) The resulting $\lambda_i^{sg}(p^2)$ are substituted into the gap equation, which is solved for complex external momenta distributed

along the boundary of the same parabolic domain while retaining the full kinematic structure of $\bar{\Gamma}_\mu$, given by Eq. (10).

(v) Steps (ii)–(iv) are repeated until convergence has been reached simultaneously for $A(p^2)$, $B(p^2)$, and the $\lambda_i^{sg}(p^2)$, with a numerical tolerance of 10^{-6} .

Following this algorithm, and using standard numerical techniques (see *e.g.*, [55]), the quark propagator and quark-gluon vertex were determined within the domain bounded by the parabola $y^2 = ax + b$, with $a = 0.6 \text{ GeV}^2$ and $b = 0.09 \text{ GeV}^4$.

4. Results

In this section we present a summary of the most prominent results of our analysis. In what follows we suppress the index “sg” throughout.

4.1. The vertex form factors in the complex plane

The soft-gluon limit of the eight form factors λ_i has been computed within the domain defined by the parabola mentioned above. In Fig. 2 we display the corresponding results for $\lambda_1(p^2)$, $\lambda_4(p^2)$ and $\lambda_7(p^2)$; this particular subset has been selected because it constitutes the dominant triplet of form factors that largely determines the bulk of the quark propagator (see Sec. 4.3).

Note that the above results agree rather well with those obtained in [32], where a fixed propagator with complex conjugate poles was employed, instead of the dynamical quark propagator (with real poles, see Sec. 4.2) used here. This suggests that the form of the $\lambda_i(p^2)$ is relative insensitive to the details of the quark propagator used for their computation.

4.2. Quark propagator: Real poles with opposite-sign residues

The most noteworthy feature of the quark propagator that emerges from this analysis is the absence of complex conjugate poles from its Dirac components $\sigma_v(p^2)$ and $\sigma_s(p^2)$, introduced in Eq. (3). This finding is in stark contradistinction to what happens within the RL and related approximations, where complex conjugate poles constitute a standard feature. Instead, in the present case, one encounters a pair of real poles, denoted by p_1^2 and p_2^2 , lying on the time-like axis, namely

$$p_1^2 = -0.16 \text{ GeV}^2, \quad p_2^2 = -0.58 \text{ GeV}^2. \quad (14)$$

Note in particular that the value of p_1^2 is in agreement with the estimate $p_1^2 \approx 1.2\mathcal{M}^2(0)$ provided in [61]. We do not find any other singularities for either the real or imaginary part being smaller than 1 GeV^2 , neither in $\sigma_v(p^2)$ nor in $\sigma_s(p^2)$.

Quite importantly, the two poles have residues with *opposite signs*: the first pole has a positive residue, whereas the second a negative one, namely

$$\text{Res}(\sigma_v, p_1^2) = 1.12, \quad \text{Res}(\sigma_v, p_2^2) = -0.51. \quad (15)$$

In order to establish that the singularities found at p_i^2 correspond to simple poles, we considered the $\lim_{z \rightarrow p_i^2} (z - p_i^2)^m f(z)$, as m is varied. A careful analysis reveals that, at a high level of accuracy, this limit is finite for $m = 1$, while it vanishes or diverges as m moves to the right or to the left of unity, respectively.

The location of the first pole, p_1^2 , is determined directly from the numerical solution of the gap equation in the complex plane; it is identified with the point where the iterative procedure ceases to converge. The existence of this pole is independently confirmed using SPM extrapolations, constructed from the data available up until that point. This SPM analysis predicts, in addition, a second pole, namely p_2^2 .

In the left panel of Fig. 3 we show the real part of $\sigma_v(p^2)$. The light-blue area indicates the domain defined by the parabola where direct numerical calculations were performed, up to the point where the first pole, p_1^2 , was reached. The pale orange surface represents the SPM extrapolation beyond this region; the appearance of a second pole, p_2^2 , pointing towards the opposite direction, is marginally visible.

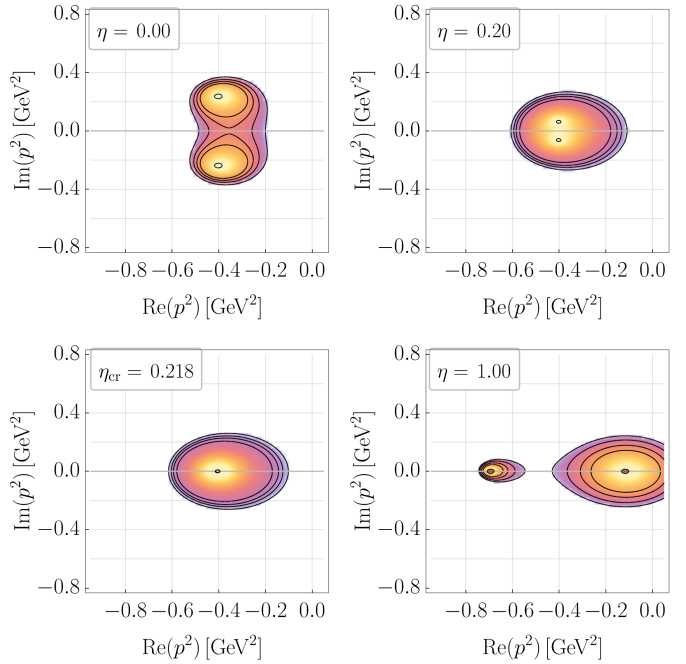


Figure 5: Contour plot of $\sigma_v(p^2)$ showing the evolution of the pole structure as the coefficient η is varied for the vertex in Eq. (16). For small η , the propagator features a pair of complex conjugate poles, which become real as η exceeds a critical value η_{cr} .

The position of p_1^2 and p_2^2 remains stable, varying by less than 5% under changes in both the data sets and the number of points used to construct the extrapolations. Moreover, in all cases, we find no evidence of clustered non-analyticities in their vicinity, supporting their interpretation as isolated singularities.

Note that both functions $A(p^2)$ and $\mathcal{M}(p^2)$ are analytic within the domain of the defining parabola. Thus, the poles observed in $\sigma_v(p^2)$ and $\sigma_s(p^2)$ originate from the zeros of the expression $p^2 + \mathcal{M}^2(p^2)$, or, equivalently, the intersection of $\mathcal{M}^2(p^2)$ with the straight line $-p^2$ (see discussion at the end of Sec. 4.3).

Given the robustness of the calculated locations, Eq. (14), and residues, Eq. (15), of these two lowest-lying poles, their physical interpretation warrants careful analysis. That of the first pole at p_1^2 is straightforward: it signals a propagating mode of a massive Dirac fermion with a dynamically generated mass of 400 MeV. The corresponding residue of the vector component $\sigma_v(p^2)$ is expected to be roughly equal to or slightly smaller than $1/A(0)$, following the discussion in [61]. According to standard field-theoretic requirements, a strict particle interpretation requires this value to remain bounded below unity [65]. While our current numerical result is slightly larger than one, this minor deviation is likely an artifact of the employed truncation approximations.

In contrast, the second pole carries a strictly negative residue, signaling the presence of an unphysical ghost state. Consequently, the associated spectral functions assume negative values, establishing that the quark propagator violates reflection positivity. Because the underlying quark states do not span a positive-definite Hilbert space, quarks are formally prohib-

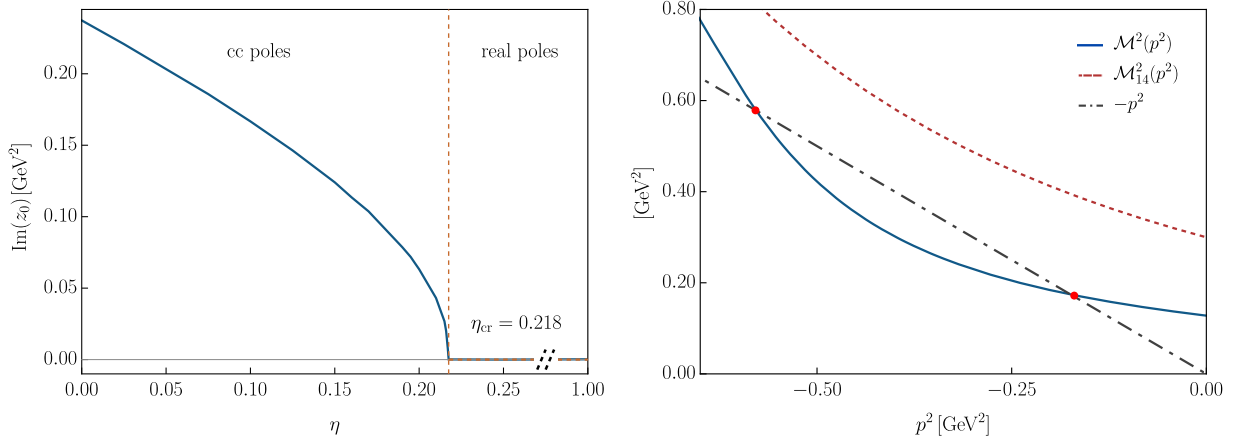


Figure 6: Left panel: Imaginary part of the quark propagator pole, z_0 , as a function of the parameter η , Eq. (16). Right panel: zeros of the function $p^2 + \mathcal{M}^2(p^2)$, for two different cases, the $\mathcal{M}^2(p^2)$ obtained with the full quark-gluon vertex active in the gap equation (blue solid curve), and the $\mathcal{M}_{14}^2(p^2)$, corresponding to the case where only the TLC and ACM components are included (red-dashed curve).

ited from appearing as asymptotic states [1, 96]. Importantly, this structural feature accommodates the scenario where quark states act as parent states within a non-perturbative BRST quartet framework [97, 98], providing a concrete, real-axis realization of a central mechanism of color confinement [99, 100].

At this point, one might speculate that the exact quark propagator in any linear covariant gauge possesses an infinite tower of poles on the time-like half-axis. These states would feature alternating-sign residues with decreasing absolute values at high $-p^2$, a mathematical configuration necessary to satisfy the axiomatic condition that the propagator vanishes as $p^2 \rightarrow \infty$ in all directions of the complex plane [96].

Independent of this conjecture, our concrete numerical results provide clear evidence that the unquenched quark propagator in the Landau gauge possesses exclusively real poles while actively violating positivity. To the best of our knowledge, this real-axis mechanism offers a fundamentally novel perspective on the functional realization of color confinement.

4.3. The interplay between ACM and SMC

In order to gain further insights on the origin of these poles, as well as the conditions that drive the transition from complex conjugate to real, we have analyzed the impact of individual form factors $\lambda_i(p^2)$ on the analytic structure of the quark propagator.

The first observation is that the combined contribution of $\lambda_1(p^2)$, $\lambda_4(p^2)$, and $\lambda_7(p^2)$ already captures the essential features of $S(p)$. The remaining five form factors produce measurable changes in the pole position, especially of p_2^2 , but do not qualitatively modify the basic picture.

We therefore focus on the analytic structure of $S(p)$ generated by the subset of form factors $\{\lambda_1, \lambda_4, \lambda_7\}$, as they are sequentially activated. To understand the distinct impact of these three form factors, it is illustrative to first examine their individual contributions to the quark propagator. To this end, the quark gap equation is solved by retaining only these specific vertex components. Remarkably, yet in complete agreement

with the recent study of [61], the TLC λ_1 provides only a minor contribution. In the upper panels of Fig. 4, the individual impacts of the TLC, ACM, and SMC on the propagator functions $B(p^2)$ and $A(p^2)$ are displayed. As clearly shown in the upper left panel, the dominant contribution to the function $B(p^2)$ —and therefore the primary mechanism driving the dynamical generation of the quark mass—originates from the ACM λ_4 . Notably, the SMC λ_7 does not contribute to $B(p^2)$ at all. Conversely, the largest contribution to the dynamical dressing of $A(p^2)$, and thus to its momentum dependence, is driven by the SMC. Therefore, the SMC form factor exerts a significant influence on the momentum dependence of $\mathcal{M}(p^2) = B(p^2)/A(p^2)$ without directly participating in the dynamical mass generation.

Together, the ACM and SMC form factors induce a distinct momentum dependence in the mass function $\mathcal{M}(p^2)$ compared to the standard result originating from the TLC alone, which is the sole component retained in the RL truncation. This difference is most apparent in the product $p^2 \mathcal{M}(p^2)$, displayed in the lower left panel of Fig. 4 alongside the corresponding quantity from an RL-truncated gap equation (black line). The dynamical part of the RL result is primarily concentrated below 2 GeV; above this threshold, the mass function exhibits a characteristic $1/p^2$ behavior with logarithmic corrections. In contrast, the results incorporating the ACM and SMC display significant dynamical contributions extending up to several GeV. Specifically, the solid red line shows $p^2 \mathcal{M}(p^2)$ with only the TLC and ACM structures retained, while the solid blue line includes the full contribution of the TLC, ACM, and SMC. Common to both curves is a drastically modified ultraviolet behavior: the dominant contribution to the mass function in the several GeV range is a $1/p^4$ term, in excellent agreement with the parametrization provided in [64] for their lattice data. Further details regarding this momentum dependence can be found in [61].

Our results, which further confirm the respective findings of [61, 64], make it evident that at Euclidean momenta around 2 GeV, the quark mass function still contains substantial non-perturbative contributions. This physical feature motivates our

quark-gluon vertex	poles	$\mathcal{M}(0)$ [MeV]
λ_1	real	180
λ_1, λ_4	cc	546
$\lambda_1, \lambda_4, \lambda_7$	real	310
all form factors	real	350

Table 1: The type of the two lowest-lying poles of the quark propagator and the value of the constituent quark mass, $\mathcal{M}(0)$, for the different sets of the quark-gluon vertex form factors retained in the gap equation (cc=complex conjugate).

choice of the renormalized mass $m_R = 50$ MeV at the renormalization scale $\mu = 2$ GeV. Deep within the perturbative domain, the mass function decreases to a few MeV, thereby accurately representing a physical up quark.

The lower right panel of Fig. 4 displays a comparison of our calculated quark mass function with the parametrization of the lattice data provided in [64]. We attribute the remaining mismatch to the use of the soft-gluon approximation within the quark-gluon vertex truncation. Nevertheless, it is evident that this momentum dependence yields a significantly closer agreement with the lattice data than the result obtained from a standard RL truncation.

Next, we analyze the impact of the individual quark-gluon vertex form factors on the locations of the two lowest-lying poles. The inclusion of the TLC λ_1 alone in the gap equation gives rise to a low value for $\mathcal{M}(0)$ of about 180 MeV, while maintaining an analytic structure characterized by two real poles. This behavior is expected from studies of the quark gap equation featuring subcritical or marginally critical couplings [31, 57]. As the ACM λ_4 is gradually introduced, dynamical mass generation increases. However, when the contribution of the ACM is turned up to approximately 35% of its full strength, the two real poles merge; for even greater strengths of the ACM, they evolve into a pair of complex conjugate poles.

The full addition of the ACM λ_4 , *i.e.*, taking into account the doublet $\{\lambda_1, \lambda_4\}$, provides sufficient strength to increase $\mathcal{M}(0)$ to 546 MeV; however, now the two lowest-lying poles evolve into a complex conjugate pair, located at z_0 and \bar{z}_0 . Then, the inclusion of λ_7 brings $\mathcal{M}(0)$ to 310 MeV, which is close to the final value of $\mathcal{M}(0) = 350$ MeV, obtained when all eight form factors are in. In addition, and most importantly, the poles of the quark propagator become real again, and remain so after the inclusion of the subleading form factors λ_i , $i = 2, 3, 5, 6, 8$.³ This general picture is succinctly summarized in Tab. 1.

In order to explore in detail the transition from the complex conjugate to real poles, we introduce an effective quark-gluon vertex, $\bar{\Gamma}_\eta^\mu$, given by

$$\bar{\Gamma}_\eta^\mu(q, p, -k) = \lambda_1^{sg}(p^2)\bar{\tau}_1^\mu + \lambda_4^{sg}(p^2)\bar{\tau}_4^\mu + \eta\lambda_7^{sg}(p^2)\bar{\tau}_7^\mu, \quad (16)$$

with $\eta \in [0, 1]$. Evidently, the extreme case $\eta = 0$ corresponds to the inclusion in the gap equation of the doublet $\{\lambda_1, \lambda_4\}$, while

$\eta = 1$ describes the impact of the full triplet $\{\lambda_1, \lambda_4, \lambda_7\}$. The role of the parameter η is to illustrate how the nature of the poles changes as one gradually increases the strength of λ_7 .

In Fig. 5 we display the pole structure of $\sigma_v(p^2)$ for four representative values of the coefficient η . As η is tuned towards its physical value, $\eta = 1$, the analytic structure undergoes a qualitative transformation.

Specifically, at $\eta = 0$ (upper-left), the contribution from $\lambda_7(p^2)$ vanishes, and the quark propagator exhibits a pair of complex conjugate poles, $z_0 = (-0.4 + 0.23i)$ GeV², and $\bar{z}_0 = (-0.4 - 0.23i)$ GeV². As η increases, thereby gradually restoring the contribution from $\lambda_7(p^2)$, the poles approach one another (upper-right). A transition occurs at the critical value $\eta_{cr} = 0.218$, where the two poles merge into a single pole of order two (lower-left). Beyond this threshold, the impact of $\lambda_7(p^2)$ becomes sufficiently strong to counteract $\lambda_4(p^2)$, driving the poles on the real axis into two separated simple poles (lower-right).

This behavior is further illustrated in the left panel of Fig. 6, where we plot the imaginary part of z_0 , denoted by $\text{Im}(z_0)$, as a function of the tuning parameter η . The $\text{Im}(z_0)$ decreases monotonically with increasing η , and vanishes exactly for $\eta = \eta_{cr}$. Past this critical point, the pole remains purely real. The resulting curve in Fig. 6 resembles the order parameter behavior in a second-order phase transition, such as, *e.g.*, temperature-dependent magnetization.

The right panel of Fig. 6 graphically displays the zeros of the propagator denominators, $p^2 + \mathcal{M}^2(p^2)$, for time-like momenta up to 0.8 GeV. Here, $\mathcal{M}_{14}(p^2)$ denotes the solution incorporating only the TLC and the ACM. This curve does not intersect the $-p^2$ line, yielding no real solution to the pole condition $p^2 + \mathcal{M}^2(p^2) = 0$. Conversely, when including the TLC, ACM, and SMC, the resulting mass function produces exactly two real zeros. Two remarks are in order regarding this mechanism: First, the drastically altered momentum behavior on the Euclidean side plays a decisive role, aligning with the analytical model for quark propagator poles provided in [61]. Second, and more importantly, the orientations of these crossings in the right panel of Fig. 6 are geometrically distinct. Consequently, the opposite signs for the residues emerge naturally from this topological analysis.

5. Conclusions

In this work we have studied the coupled system of functional equations that describes the up quark propagator and the quark-gluon vertex in the complex plane. The structure of the vertex SDE employed is dictated by the symmetry-preserving approach developed in [73–75], and furnishes the momentum evolution of all eight vertex form factors, in the Landau gauge. The analysis is simplified by evaluating these form factors in the soft-gluon limit, where they become a function of a single kinematic variable.

Our numerical results indicate that the nature of the poles in the quark propagator depends crucially on the structure of the quark-gluon vertex employed in the gap equation. When the

³Note that the present described mechanism verifies a conjecture recently formulated in [31].

kernel is composed solely of the “classical” component λ_1 , the dynamical mass generation is much too weak, and the quark propagator displays two low-lying real poles, typical of subcritical or marginally critical coupling strengths.

With a kernel containing the “classical” and the “anomalous chromomagnetic moment” components, λ_1 and λ_4 , the quark propagator develops complex conjugate poles. Instead, when the kernel receives contributions also from the “spin-momentum curvature” component, λ_7 , the poles become real again, possessing residues with opposite algebraic signs. This characteristic structure persists even after all remaining form factors have been included into the gap equation.

The alternating signs of the residues imply a positivity-violating quark propagator, a direct consequence of the negative domains induced in the spectral function by the ghost pole. Consequently, the space of quark states is not positive-definite. This formally precludes the possibility of quarks acting as BRST singlets, requiring them instead to be part of a non-perturbative BRST quartet [1]. This structural mechanism constitutes a core aspect of color confinement.

Future extensions, most notably moving beyond the soft-gluon limit in the evaluation of the quark-gluon vertex form factors, are planned to further corroborate and elucidate the insights obtained here into the analytic structure of the quark propagator. Furthermore, implications for hadron physics will be investigated to seek empirical evidence for these quark-level mechanisms. In this respect, it would be highly interesting to explore whether the framework presented here can serve as a firm foundation for understanding the phenomenologically successful 3P_0 model of meson decays, as suggested by the discussion in [101].

Acknowledgments

A.S.M., J.M.M. and J.P. are funded by the Spanish MICINN grants PID2020-113334GB-I00 and PID2023-151418NB-I00, the Generalitat Valenciana grant CIPROM/2022/66, and CEX2023-001292-S by MCIU/AEI. J.M.M. also acknowledges support from UV and Banco Santander, S.A. (Santander Investigación Postdoctoral program). The computations have been carried out at the CEAFCM and UHU High Performance Computer (HPC@UHU), funded by FEDER/MINECO project UNHU-15CE-2848, and on the General Computing Infrastructure (GLUON) of the UV.

References

- [1] R. Alkofer, L. von Smekal, Phys. Rept. 353 (2001) 281. doi:[10.1016/S0370-1573\(01\)00010-2](https://doi.org/10.1016/S0370-1573(01)00010-2).
- [2] J. M. Pawłowski, D. F. Litim, S. Nedelko, L. von Smekal, Phys. Rev. Lett. 93 (2004) 152002. doi:[10.1103/PhysRevLett.93.152002](https://doi.org/10.1103/PhysRevLett.93.152002).
- [3] D. Binosi, J. Papavassiliou, Phys. Rept. 479 (2009) 1–152. doi:[10.1016/j.physrep.2009.05.001](https://doi.org/10.1016/j.physrep.2009.05.001).
- [4] A. Maas, Phys. Rept. 524 (2013) 203–300. doi:[10.1016/j.physrep.2012.11.002](https://doi.org/10.1016/j.physrep.2012.11.002).
- [5] I. C. Cloet, C. D. Roberts, Prog. Part. Nucl. Phys. 77 (2014) 1–69. doi:[10.1016/j.pnpnp.2014.02.001](https://doi.org/10.1016/j.pnpnp.2014.02.001).
- [6] M. Q. Huber, Phys. Rept. 879 (2020) 1–92. doi:[10.1016/j.physrep.2020.04.004](https://doi.org/10.1016/j.physrep.2020.04.004).
- [7] N. Dupuis, L. Canet, A. Eichhorn, W. Metzner, J. M. Pawłowski, M. Tissier, N. Wschebor, Phys. Rept. 910 (2021) 1–114. doi:[10.1016/j.physrep.2021.01.001](https://doi.org/10.1016/j.physrep.2021.01.001).
- [8] M. N. Ferreira, J. Papavassiliou, Particles 6 (2023) 312–363. doi:[10.3390/particles6010017](https://doi.org/10.3390/particles6010017).
- [9] M. N. Ferreira, J. Papavassiliou, Prog. Part. Nucl. Phys. 144 (2025) 104186. doi:[10.1016/j.pnpnp.2025.104186](https://doi.org/10.1016/j.pnpnp.2025.104186).
- [10] M. Q. Huber, 2025. [arXiv:2510.18960](https://arxiv.org/abs/2510.18960).
- [11] R. Alkofer, W. Detmold, C. S. Fischer, P. Maris, Phys. Rev. D 70 (2004) 014014. doi:[10.1103/PhysRevD.70.014014](https://doi.org/10.1103/PhysRevD.70.014014).
- [12] S. Strauss, C. S. Fischer, C. Kellermann, Phys. Rev. Lett. 109 (2012) 252001. doi:[10.1103/PhysRevLett.109.252001](https://doi.org/10.1103/PhysRevLett.109.252001).
- [13] T. Frederico, G. Salmè, M. Viviani, Phys. Rev. D 89 (2014) 016010. doi:[10.1103/PhysRevD.89.016010](https://doi.org/10.1103/PhysRevD.89.016010).
- [14] D. Dudal, O. Oliveira, P. J. Silva, Phys. Rev. D 89 (2014) 014010. doi:[10.1103/PhysRevD.89.014010](https://doi.org/10.1103/PhysRevD.89.014010).
- [15] W. de Paula, T. Frederico, G. Salmè, M. Viviani, Phys. Rev. D 94 (2016) 071901. doi:[10.1103/PhysRevD.94.071901](https://doi.org/10.1103/PhysRevD.94.071901).
- [16] B. El-Bennich, G. Krein, E. Rojas, F. E. Serna, Few Body Syst. 57 (2016) 955–963. doi:[10.1007/s00601-016-1133-x](https://doi.org/10.1007/s00601-016-1133-x).
- [17] R.-A. Tripolt, P. Gubler, M. Ulybyshev, L. Von Smekal, Comput. Phys. Commun. 237 (2019) 129–142. doi:[10.1016/j.cpc.2018.11.012](https://doi.org/10.1016/j.cpc.2018.11.012).
- [18] D. Binosi, R.-A. Tripolt, Phys. Lett. B 801 (2020) 135171. doi:[10.1016/j.physletb.2019.135171](https://doi.org/10.1016/j.physletb.2019.135171).
- [19] D. Dudal, O. Oliveira, M. Roelfs, P. Silva, Nucl. Phys. B 952 (2020) 114912. doi:[10.1016/j.nucphysb.2019.114912](https://doi.org/10.1016/j.nucphysb.2019.114912).
- [20] G. Eichmann, P. Duarte, M. T. Peña, A. Stadler, Phys. Rev. D 100 (2019) 094001. doi:[10.1103/PhysRevD.100.094001](https://doi.org/10.1103/PhysRevD.100.094001).
- [21] S. W. Li, P. Lowdon, O. Oliveira, P. J. Silva, Phys. Lett. B 803 (2020) 135329. doi:[10.1016/j.physletb.2020.135329](https://doi.org/10.1016/j.physletb.2020.135329).

- [22] S. W. Li, P. Lowdon, O. Oliveira, P. J. Silva, *Phys. Lett. B* 823 (2021) 136753. doi:[10.1016/j.physletb.2021.136753](https://doi.org/10.1016/j.physletb.2021.136753).
- [23] C. S. Fischer, M. Q. Huber, *Phys. Rev. D* 102 (2020) 094005. doi:[10.1103/PhysRevD.102.094005](https://doi.org/10.1103/PhysRevD.102.094005).
- [24] J. Horak, J. Papavassiliou, J. M. Pawłowski, N. Wink, *Phys. Rev. D* 104 (2021) 074017. doi:[10.1103/PhysRevD.104.074017](https://doi.org/10.1103/PhysRevD.104.074017).
- [25] J. Horak, J. M. Pawłowski, J. Rodríguez-Quintero, J. Turnwald, J. M. Urban, N. Wink, S. Zafeiropoulos, *Phys. Rev. D* 105 (2022) 036014. doi:[10.1103/PhysRevD.105.036014](https://doi.org/10.1103/PhysRevD.105.036014).
- [26] J. Horak, J. M. Pawłowski, N. Wink, *SciPost Phys. Core* 8 (2025) 048. doi:[10.21468/SciPostPhysCore.8.3.048](https://doi.org/10.21468/SciPostPhysCore.8.3.048).
- [27] G. Eichmann, E. Ferreira, A. Stadler, *Phys. Rev. D* 105 (2022) 034009. doi:[10.1103/PhysRevD.105.034009](https://doi.org/10.1103/PhysRevD.105.034009).
- [28] J. Horak, J. M. Pawłowski, N. Wink, *SciPost Phys.* 15 (2023) 149. doi:[10.21468/SciPostPhys.15.4.149](https://doi.org/10.21468/SciPostPhys.15.4.149).
- [29] M. Q. Huber, W. J. Kern, R. Alkofer, *Phys. Rev. D* 107 (2023) 074026. doi:[10.1103/PhysRevD.107.074026](https://doi.org/10.1103/PhysRevD.107.074026).
- [30] M. Q. Huber, W. J. Kern, R. Alkofer, *Symmetry* 15 (2023) 414. doi:[10.3390/sym15020414](https://doi.org/10.3390/sym15020414).
- [31] J. M. Pawłowski, J. Wessely, *Eur. Phys. J. C* 85 (2025) 970. doi:[10.1140/epjc/s10052-025-14683-z](https://doi.org/10.1140/epjc/s10052-025-14683-z).
- [32] M. N. Ferreira, A. S. Miramontes, J. M. Morgado, J. Papavassiliou (2026). [arXiv:2605.06242](https://arxiv.org/abs/2605.06242).
- [33] P. Maris, P. C. Tandy, *Phys. Rev. C* 61 (2000) 045202. doi:[10.1103/PhysRevC.61.045202](https://doi.org/10.1103/PhysRevC.61.045202).
- [34] P. Maris, P. C. Tandy, *Phys. Rev. C* 62 (2000) 055204. doi:[10.1103/PhysRevC.62.055204](https://doi.org/10.1103/PhysRevC.62.055204). [arXiv:nuc1-th/0005015](https://arxiv.org/abs/nuc1-th/0005015).
- [35] S. R. Cotanch, P. Maris, *Phys. Rev. D* 68 (2003) 036006. doi:[10.1103/PhysRevD.68.036006](https://doi.org/10.1103/PhysRevD.68.036006). [arXiv:nuc1-th/0308008](https://arxiv.org/abs/nuc1-th/0308008).
- [36] D. Nicmorus, G. Eichmann, A. Krassnigg, R. Alkofer, *Phys. Rev. D* 80 (2009) 054028. doi:[10.1103/PhysRevD.80.054028](https://doi.org/10.1103/PhysRevD.80.054028).
- [37] T. Hilger, M. Gomez-Rocha, A. Krassnigg, *Phys. Rev. D* 91 (2015) 114004. doi:[10.1103/PhysRevD.91.114004](https://doi.org/10.1103/PhysRevD.91.114004).
- [38] T. Hilger, C. Popovici, M. Gomez-Rocha, A. Krassnigg, *Phys. Rev. D* 91 (2015) 034013. doi:[10.1103/PhysRevD.91.034013](https://doi.org/10.1103/PhysRevD.91.034013).
- [39] G. Eichmann, H. Sanchis-Alepuz, R. Williams, R. Alkofer, C. S. Fischer, *Prog. Part. Nucl. Phys.* 91 (2016) 1–100. doi:[10.1016/j.ppnp.2016.07.001](https://doi.org/10.1016/j.ppnp.2016.07.001).
- [40] F. F. Mojica, C. E. Vera, E. Rojas, B. El-Bennich, *Phys. Rev. D* 96 (2017) 014012. doi:[10.1103/PhysRevD.96.014012](https://doi.org/10.1103/PhysRevD.96.014012).
- [41] H. Sanchis-Alepuz, R. Alkofer, C. S. Fischer, *Eur. Phys. J. A* 54 (2018) 41. doi:[10.1140/epja/i2018-12465-x](https://doi.org/10.1140/epja/i2018-12465-x).
- [42] E. Weil, G. Eichmann, C. S. Fischer, R. Williams, *Phys. Rev. D* 96 (2017) 014021. doi:[10.1103/PhysRevD.96.014021](https://doi.org/10.1103/PhysRevD.96.014021).
- [43] F. E. Serna, B. El-Bennich, G. Krein, *Phys. Rev. D* 96 (2017) 014013. doi:[10.1103/PhysRevD.96.014013](https://doi.org/10.1103/PhysRevD.96.014013).
- [44] P. C. Wallbott, G. Eichmann, C. S. Fischer, *Phys. Rev. D* 100 (2019) 014033. doi:[10.1103/PhysRevD.100.014033](https://doi.org/10.1103/PhysRevD.100.014033).
- [45] N. Santowsky, G. Eichmann, C. S. Fischer, P. C. Wallbott, R. Williams, *Phys. Rev. D* 102 (2020) 056014. doi:[10.1103/PhysRevD.102.056014](https://doi.org/10.1103/PhysRevD.102.056014).
- [46] Á. Miramontes, A. Bashir, K. Raya, P. Roig, *Phys. Rev. D* 105 (2022) 074013. doi:[10.1103/PhysRevD.105.074013](https://doi.org/10.1103/PhysRevD.105.074013).
- [47] F. Gao, A. S. Miramontes, J. Papavassiliou, J. M. Pawłowski, *Phys. Lett. B* 863 (2025) 139384. doi:[10.1016/j.physletb.2025.139384](https://doi.org/10.1016/j.physletb.2025.139384).
- [48] Y.-Z. Xu, *JHEP* 2024 (2024) 118. doi:[10.1007/JHEP07\(2024\)118](https://doi.org/10.1007/JHEP07(2024)118).
- [49] J. Hoffer, G. Eichmann, C. S. Fischer, *Phys. Rev. D* 111 (2025) 054028. doi:[10.1103/PhysRevD.111.054028](https://doi.org/10.1103/PhysRevD.111.054028).
- [50] G. Eichmann, 2025. [arXiv:2503.10397](https://arxiv.org/abs/2503.10397).
- [51] S. Hage, C. S. Fischer, M. Q. Huber, J. Y. Yigzaw, 2025. [arXiv:2510.27423](https://arxiv.org/abs/2510.27423).
- [52] C. Shi, L. Lu, I. C. Cloët, W. Jia, P. C. Tandy, *Phys. Rev. D* 113 (2026) L111501. doi:[10.1103/yklv-ntq9](https://doi.org/10.1103/yklv-ntq9).
- [53] C. S. Fischer, D. Nickel, R. Williams, *Eur. Phys. J. C* 60 (2009) 47–61. doi:[10.1140/epjc/s10052-008-0821-1](https://doi.org/10.1140/epjc/s10052-008-0821-1).
- [54] A. Windisch, *Phys. Rev. C* 95 (2017) 045204. doi:[10.1103/PhysRevC.95.045204](https://doi.org/10.1103/PhysRevC.95.045204). [arXiv:1612.06002](https://arxiv.org/abs/1612.06002).
- [55] H. Sanchis-Alepuz, R. Williams, *Comput. Phys. Commun.* 232 (2018) 1–21. doi:[10.1016/j.cpc.2018.05.020](https://doi.org/10.1016/j.cpc.2018.05.020).
- [56] Á. S. Miramontes, H. Sanchis-Alepuz, *Eur. Phys. J. A* 55 (2019) 170. doi:[10.1140/epja/i2019-12847-6](https://doi.org/10.1140/epja/i2019-12847-6).

- [57] R. Alkofer, C. S. Fischer, F. Zierler, Phys. Rev. D 113 (2026) 094002. doi:[10.1103/q3kq-s8qn](https://doi.org/10.1103/q3kq-s8qn).
- [58] P. Maris, P. C. Tandy, Phys. Rev. C 60 (1999) 055214. doi:[10.1103/PhysRevC.60.055214](https://doi.org/10.1103/PhysRevC.60.055214).
- [59] L. Chang, C. D. Roberts, Phys. Rev. Lett. 103 (2009) 081601. doi:[10.1103/PhysRevLett.103.081601](https://doi.org/10.1103/PhysRevLett.103.081601).
- [60] K.-I. Kondo, M. Murakami, Phys. Rev. D 101 (2020) 074044.
- [61] G. Wieland, R. Alkofer, 2026. [arXiv:2604.20235](https://arxiv.org/abs/2604.20235).
- [62] L. Chang, Y.-X. Liu, C. D. Roberts, Phys. Rev. Lett. 106 (2011) 072001. doi:[10.1103/PhysRevLett.106.072001](https://doi.org/10.1103/PhysRevLett.106.072001).
- [63] D. Binosi, L. Chang, J. Papavassiliou, S.-X. Qin, C. D. Roberts, Phys. Rev. D 95 (2017) 031501. doi:[10.1103/PhysRevD.95.031501](https://doi.org/10.1103/PhysRevD.95.031501).
- [64] O. Oliveira, T. Frederico, W. de Paula, Eur. Phys. J. C 85 (2025) 280. doi:[10.1140/epjc/s10052-025-13984-7](https://doi.org/10.1140/epjc/s10052-025-13984-7).
- [65] C. Itzykson, J. B. Zuber, Quantum Field Theory, International Series in Pure and Applied Physics, New York, USA: McGraw-Hill (1980) 705 p., 1980.
- [66] A. C. Aguilar, M. N. Ferreira, B. M. Oliveira, J. Papavassiliou, G. T. Linhares, Eur. Phys. J. C 84 (2024) 1231. doi:[10.1140/epjc/s10052-024-13605-9](https://doi.org/10.1140/epjc/s10052-024-13605-9).
- [67] R. Alkofer, C. S. Fischer, F. J. Llanes-Estrada, K. Schwenzer, Annals Phys. 324 (2009) 106–172. doi:[10.1016/j.aop.2008.07.001](https://doi.org/10.1016/j.aop.2008.07.001).
- [68] R. Williams, C. S. Fischer, W. Heupel, Phys. Rev. D 93 (2016) 034026. doi:[10.1103/PhysRevD.93.034026](https://doi.org/10.1103/PhysRevD.93.034026).
- [69] J. Cornwall, R. Norton, Phys. Rev. D 8 (1973) 3338–3346. doi:[10.1103/PhysRevD.8.3338](https://doi.org/10.1103/PhysRevD.8.3338).
- [70] J. M. Cornwall, R. Jackiw, E. Tomboulis, Phys. Rev. D 10 (1974) 2428–2445. doi:[10.1103/PhysRevD.10.2428](https://doi.org/10.1103/PhysRevD.10.2428).
- [71] J. Berges, Phys. Rev. D 70 (2004) 105010. doi:[10.1103/PhysRevD.70.105010](https://doi.org/10.1103/PhysRevD.70.105010).
- [72] M. E. Carrington, Y. Guo, Phys. Rev. D 83 (2011) 016006. doi:[10.1103/PhysRevD.83.016006](https://doi.org/10.1103/PhysRevD.83.016006).
- [73] A. S. Miramontes, J. M. Morgado, J. Papavassiliou, J. M. Pawłowski, Eur. Phys. J. C 85 (2025) 1055. doi:[10.1140/epjc/s10052-025-14774-x](https://doi.org/10.1140/epjc/s10052-025-14774-x).
- [74] M. N. Ferreira, A. S. Miramontes, J. M. Morgado, J. Papavassiliou, J. M. Pawłowski, Eur. Phys. J. C 86 (2026) 325. doi:[10.1140/epjc/s10052-026-15487-5](https://doi.org/10.1140/epjc/s10052-026-15487-5).
- [75] M. N. Ferreira, A. S. Miramontes, M. J. M., J. Papavassiliou, 2026. [arXiv:2604.07221](https://arxiv.org/abs/2604.07221).
- [76] G. Eichmann, R. Williams, R. Alkofer, M. Vujanovic, Phys. Rev. D 89 (2014) 105014. doi:[10.1103/PhysRevD.89.105014](https://doi.org/10.1103/PhysRevD.89.105014).
- [77] A. Blum, M. Q. Huber, M. Mitter, L. von Smekal, Phys. Rev. D 89 (2014) 061703. doi:[10.1103/PhysRevD.89.061703](https://doi.org/10.1103/PhysRevD.89.061703).
- [78] M. Q. Huber, Phys. Rev. D 93 (2016) 085033. doi:[10.1103/PhysRevD.93.085033](https://doi.org/10.1103/PhysRevD.93.085033).
- [79] M. Q. Huber, Phys. Rev. D 101 (2020) 114009. doi:[10.1103/PhysRevD.101.114009](https://doi.org/10.1103/PhysRevD.101.114009).
- [80] F. Pinto-Gómez, F. De Soto, M. N. Ferreira, J. Papavassiliou, J. Rodríguez-Quintero, Phys. Lett. B 838 (2023) 137737. doi:[10.1016/j.physletb.2023.137737](https://doi.org/10.1016/j.physletb.2023.137737).
- [81] A. C. Aguilar, M. N. Ferreira, J. Papavassiliou, L. R. Santos, Eur. Phys. J. C 83 (2023) 549. doi:[10.1140/epjc/s10052-023-11732-3](https://doi.org/10.1140/epjc/s10052-023-11732-3).
- [82] F. Pinto-Gómez, F. De Soto, J. Rodríguez-Quintero, Phys. Rev. D 110 (2024) 014005. doi:[10.1103/PhysRevD.110.014005](https://doi.org/10.1103/PhysRevD.110.014005).
- [83] A. C. Aguilar, M. N. Ferreira, D. Ibañez, J. Papavassiliou, Eur. Phys. J. C 83 (2023) 967. doi:[10.1140/epjc/s10052-023-12103-8](https://doi.org/10.1140/epjc/s10052-023-12103-8).
- [84] W. Celmaster, R. J. Gonsalves, Phys. Rev. D 20 (1979) 1420. doi:[10.1103/PhysRevD.20.1420](https://doi.org/10.1103/PhysRevD.20.1420).
- [85] A. Hasenfratz, P. Hasenfratz, Phys. Lett. B 93 (1980) 165. doi:[10.1016/0370-2693\(80\)90118-5](https://doi.org/10.1016/0370-2693(80)90118-5).
- [86] E. Braaten, J. P. Leveille, Phys. Rev. D 24 (1981) 1369. doi:[10.1103/PhysRevD.24.1369](https://doi.org/10.1103/PhysRevD.24.1369).
- [87] J. Skullerud, A. Kizilersu, J. High Energy Phys. 2002 (2002) 013. doi:[10.1088/1126-6708/2002/09/013](https://doi.org/10.1088/1126-6708/2002/09/013).
- [88] L. von Smekal, K. Maltman, A. Sternbeck, Phys. Lett. B 681 (2009) 336–342. doi:[10.1016/j.physletb.2009.10.030](https://doi.org/10.1016/j.physletb.2009.10.030).
- [89] A. Kizilersü, O. Oliveira, P. J. Silva, J.-I. Skullerud, A. Sternbeck, Phys. Rev. D 103 (2021) 114515. doi:[10.1103/PhysRevD.103.114515](https://doi.org/10.1103/PhysRevD.103.114515).
- [90] C. S. Fischer, R. Alkofer, Phys. Rev. D 67 (2003) 094020. doi:[10.1103/PhysRevD.67.094020](https://doi.org/10.1103/PhysRevD.67.094020).
- [91] A. C. Aguilar, J. Papavassiliou, Phys. Rev. D 83 (2011) 014013. doi:[10.1103/PhysRevD.83.014013](https://doi.org/10.1103/PhysRevD.83.014013).
- [92] A. C. Aguilar, J. C. Cardona, M. N. Ferreira, J. Papavassiliou, Phys. Rev. D 98 (2018) 014002. doi:[10.1103/PhysRevD.98.014002](https://doi.org/10.1103/PhysRevD.98.014002).

- [93] A. Ayala, A. Bashir, D. Binosi, M. Cristoforetti, J. Rodríguez-Quintero, *Phys. Rev. D* 86 (2012) 074512. doi:[10.1103/PhysRevD.86.074512](https://doi.org/10.1103/PhysRevD.86.074512).
- [94] D. Binosi, C. D. Roberts, J. Rodríguez-Quintero, *Phys. Rev. D* 95 (2017) 114009. doi:[10.1103/PhysRevD.95.114009](https://doi.org/10.1103/PhysRevD.95.114009).
- [95] A. C. Aguilar, F. De Soto, M. N. Ferreira, J. Papavassiliou, J. Rodríguez-Quintero, S. Zafeiropoulos, *Eur. Phys. J. C* 80 (2020) 154. doi:[10.1140/epjc/s10052-020-7741-0](https://doi.org/10.1140/epjc/s10052-020-7741-0).
- [96] R. Oehme, *Int. J. Mod. Phys. A* 10 (1995) 1995–2014. doi:[10.1142/S0217751X95000978](https://doi.org/10.1142/S0217751X95000978).
- [97] N. Alkofer, R. Alkofer, *PoS FACESQCD* (2010) 043. doi:[10.22323/1.117.0043](https://doi.org/10.22323/1.117.0043).
- [98] N. Alkofer, R. Alkofer, *Phys. Lett. B* 702 (2011) 158–163. doi:[10.1016/j.physletb.2011.06.073](https://doi.org/10.1016/j.physletb.2011.06.073).
- [99] T. Kugo, I. Ojima, *Prog. Theor. Phys. Suppl.* 66 (1979) 1–130. doi:[10.1143/PTPS.66.1](https://doi.org/10.1143/PTPS.66.1).
- [100] R. Alkofer, J. Greensite, *J. Phys. G* 34 (2007) S3. doi:[10.1088/0954-3899/34/7/S02](https://doi.org/10.1088/0954-3899/34/7/S02).
[arXiv:hep-ph/0610365](https://arxiv.org/abs/hep-ph/0610365).
- [101] R. Alkofer, F. J. Llanes-Estrada, A. Salas-Bernardez, *Phys. Rev. D* 109 (2024) 074015. doi:[10.1103/PhysRevD.109.074015](https://doi.org/10.1103/PhysRevD.109.074015).